



HAL
open science

New Shear Actuated Smart Structure Beam Finite Element

A. Benjeddou, Marcelo Areias Trindade, Roger Ohayon

► **To cite this version:**

A. Benjeddou, Marcelo Areias Trindade, Roger Ohayon. New Shear Actuated Smart Structure Beam Finite Element. *AIAA Journal*, 1999, 37 (3), pp.378–383. 10.2514/2.719 . hal-04114354

HAL Id: hal-04114354

<https://hal.science/hal-04114354>

Submitted on 15 Sep 2023

HAL is a multi-disciplinary open access archive for the deposit and dissemination of scientific research documents, whether they are published or not. The documents may come from teaching and research institutions in France or abroad, or from public or private research centers.

L'archive ouverte pluridisciplinaire **HAL**, est destinée au dépôt et à la diffusion de documents scientifiques de niveau recherche, publiés ou non, émanant des établissements d'enseignement et de recherche français ou étrangers, des laboratoires publics ou privés.

New Shear Actuated Smart Structure Beam Finite Element

A. Benjeddou,* M. A. Trindade,† and R. Ohayon‡

Conservatoire National des Arts et Métiers, F-75003 Paris, France

We present the formulation and validation of a new adaptive sandwich-beam finite element, capable of dealing with either extension or shear actuation mechanisms, which is reached by coating an elastic core with piezoelectric sheets or sandwiching a piezoelectric core between two elastic faces. The poling direction is taken parallel to the transversely applied electric field for the first mechanism and in the axial direction for the second one. The sandwich construction is made of asymmetric thin faces (Euler–Bernoulli beams) and a relatively thick core (Timoshenko beam). The obtained two-node finite element has only four mechanical degrees of freedom that are the deflection and its derivative and the mean and relative axial displacements of the faces midplanes. Finite element analysis of segmented and continuous cantilever adaptive sandwich beams with active faces (extension actuated) or core (shear actuated) show good comparisons with results found in the literature. Additional parametric studies (actuator’s position and thickness, structure’s stiffness) with the present element indicate that the shear actuation mechanism presents several promising features over the conventional extension actuation mechanism. In fact, the shear actuation mechanism is better than the extension one for stiff structures and thick piezoelectric actuators.

Introduction

RECENT and current research efforts in the field of structural control using active materials are directed toward improvements of the actuation capacity of these systems. Conventional monolithic piezoelectric actuators produce longitudinal stresses or strains through their stress-induced e_{31} or strain-induced d_{31} piezoelectric constants. Their models are based on a priori assumptions of through-thickness constant applied electric field and uniform poling and inplane constant stress or strain behavior. Using interdigitated electrodes (IDE), transverse actuation through e_{33} or d_{33} piezoelectric constants also can be introduced.¹ However, a complex poling pattern results in the actuator because of an induced in-plane component of the electric field, which must be accounted for in any model.

By sandwiching a lead zirconate titanate (PZT) layer between off-axis laminae, the composite laminate can produce twisting deformation^{2,3} through transformed piezoelectric constants \tilde{e}_{36} or \tilde{d}_{36} , but this twisting is secondary because it is caused by the extension-twisting coupling. This twisting also can be achieved through special piezoelectric attachment techniques, electrode designs,⁴ or piezoelectric fiber composites (PFC) with⁵ or without¹ interdigitated electrodes (IDEPFC).

All of the preceding advanced techniques are based essentially on the extension actuation mechanism of the piezoelectric materials because the electric field and poling vectors are always parallel, and the inherent shear effects of the material are always neglected. Hence, the e_{15} or d_{15} piezoelectric constants are not used by the preceding advanced actuators. To be used, these constants require constant electric fields, but they must be perpendicular to the poling vector. Although mentioned early in the 1990s,⁶ shear-based actuators were proposed only recently through a preliminary study with a commercial finite element analysis code⁷ and a theoretical model.⁸ A finite element model was also proposed by Benjeddou et al.^{9–11} and used to compare both extension and shear actuation mechanisms.¹² These theoretical and numerical models used the stress-induced piezoelectric coupling constant e_{15} of an axially poled PZT layer or a patch sandwiched between thin elastic layers.

The d_{15} -based torsional actuators also were proposed recently for the production of large angular displacement and torque.¹³ Actuator designs and assembly methods, materials preparation, poling procedures, test results for joint strengths, and actuator output capabilities are discussed. This report pointed out that the current commercially available PZT piezoceramics are not optimized for their shear piezoelectric response and that most of the current PZT piezoceramics are optimized for their extension piezoelectric properties.

The objective of this paper is to present a new adaptive sandwich-beam finite element capable of dealing with either extension or shear actuation mechanisms. A new mechanical model is proposed to avoid shear locking present in the previous element.^{9–11} This model is based on the use of mean and relative axial displacements of the midplanes of the faces, instead of those of the upper and lower skins of the core used in the previous element. An extra-shear strain due to the faces sliding against the core is then induced, and all quantities are expressed in terms of the faces’ displacements. In the following sections theoretical and finite element (FE) models are presented and then validated through static and free-vibration analysis of various cantilevered adaptive beam configurations. Results are compared to the numerical and analytic results found in the literature. Conclusions and prospects are then formulated at the end of the paper.

Theoretical Model

Consider a sandwich beam made of either piezoelectric surface layers and elastic core or piezoelectric core and elastic surface layers. In the first configuration the surface layers are poled transversely, whereas in the second one the core is axially poled. For both cases a through-thickness electric field is applied to each piezoelectric layer. However, elastic layers are assumed insulated. All layers are assumed to be perfectly bonded and in the xz plane deformation state. The Bernoulli–Euler theory is retained for the sandwich-beam surface layers, whereas the core is assumed to behave as a Timoshenko beam. A local frame is attached to each layer at its left-end center, whereas the global one is located at the left-end center of the whole beam, so that the beam’s centroidal and elastic axes coincide with the x axis. The length, width, and thickness of the beam are denoted by L , b , and h , respectively. A , B , and C indices indicate top, bottom, and core layer quantities, and the F index is used for surface-layer parameters.

Mechanical Displacements

Starting with linear axial displacements for each layer and enforcing the interface displacement continuities leads to the following expressions for the axial displacements for the faces and the core, respectively:

* Research Assistant Professor, Structural Mechanics and Coupled Systems Laboratory. Member AIAA.

† Doctoral Student, Structural Mechanics and Coupled Systems Laboratory.

‡ Professor, Structural Mechanics and Coupled Systems Laboratory.

$$u_i = \left(\bar{u} \pm \frac{\tilde{u}}{2} \right) - (z - z_i)w', \quad i = A(+), B(-)$$

$$u_C = (\bar{u} + dw') + z \left(\frac{\tilde{u}}{h_C} + \lambda w' \right) \quad (1)$$

$$d = \frac{h_A - h_B}{4}, \quad \lambda = \frac{h_A + h_B}{2h_C}$$

where w' is the first derivative of the transverse deflection (constant through-thickness). Variables \bar{u} and \tilde{u} are the mean and relative axial displacements of the upper and lower sandwich-beam faces, defined by

$$\bar{u} = \frac{\bar{u}_A + \bar{u}_B}{2}, \quad \tilde{u} = \bar{u}_A - \bar{u}_B \quad (2)$$

where \bar{u}_A and \bar{u}_B are midplane displacements of the upper and lower surface layers.

The geometrical parameter d couples the bending behavior of the surface layers to the membrane behavior of the core and vanishes for symmetrical sandwich construction. However, the mechanical parameter λ , coupling the bending behavior of the surface layers to that of the core, is intrinsic because it does not vanish even for symmetrical construction and is an important variable for parameter studies.

Reduced Constitutive Equations

A linear orthotropic piezoelectric material with material symmetry axes parallel to the beam axes is considered for piezoelectric layers; c_{ij} , e_{kj} , and ϵ_k ($i, j = 1, \dots, 6$; $k = 1, 2, 3$) denote its elastic, piezoelectric, and dielectric constants, respectively.

For the extension actuation mechanism, the piezoelectric beam surface layers are poled parallel to the through-thickness applied electric field. Using the preceding mechanical assumptions, the three-dimensional linear constitutive equations of an orthotropic piezoelectric layer can be reduced^{9,11} to

$$\begin{Bmatrix} \sigma_1 \\ D_3 \end{Bmatrix} = \begin{bmatrix} c_{11}^* & -e_{31}^* \\ e_{31}^* & \epsilon_3^* \end{bmatrix} \begin{Bmatrix} \epsilon_1 \\ E_3 \end{Bmatrix}, \quad c_{11}^* = c_{11} - \frac{c_{13}^2}{c_{33}} \quad (3)$$

$$e_{31}^* = e_{31} - \frac{c_{13}}{c_{33}}e_{33}, \quad \epsilon_3^* = \epsilon_3 + \frac{e_{33}^2}{c_{33}}$$

where σ_1 , ϵ_1 , D_3 , and E_3 are axial stress and strain and transverse electric displacement and field. Notice that the electromechanical coupling is between axial strain and transverse electric field only, which is the basic foundation of the extension actuation mechanism.

For the shear actuation mechanism, the piezoelectric core layer is poled in the axial direction, i.e., perpendicular to the applied transverse electric field. Applying coordinate transformations^{1,3} so that the axial and transverse indices interchange and using the preceding mechanical assumptions, the three-dimensional linear constitutive equations of the orthotropic piezoelectric core reduce to^{9,11}

$$\begin{Bmatrix} \sigma_1 \\ \sigma_5 \\ D_3 \end{Bmatrix} = \begin{bmatrix} c_{33}^* & 0 & 0 \\ 0 & c_{55} & -e_{15} \\ 0 & e_{15} & \epsilon_1 \end{bmatrix} \begin{Bmatrix} \epsilon_1 \\ \epsilon_5 \\ E_3 \end{Bmatrix}, \quad c_{33}^* = c_{33} - \frac{c_{13}^2}{c_{11}} \quad (4)$$

where σ_5 and ϵ_5 are the transverse shear stress and strain. Notice also that the electromechanical coupling is between shear strain and transverse electric field only; this is the origin of the newly defined concept of the shear actuation mechanism.

Electric Potentials

Electric potential patterns in each piezoelectric layer for each actuation mechanism are obtained through a combination of Eqs. (1) and (2) and the corresponding reduced constitutive equation (3) or (4) and then an integration of the electrostatic equilibrium equation ignoring free volumic charge density.

For the extension actuation mechanism, integration of the reduced electrostatic equilibrium equation

$$D_{i3,3} = 0, \quad i = A, B \quad (5)$$

leads to the following electric potentials in the faces:

$$\varphi_i = \bar{\varphi}_i + (z - z_i) \frac{\tilde{\varphi}_i}{h_i} + \left[1 - \frac{4(z - z_i)^2}{h_i^2} \right] \frac{h_i^2}{8} \frac{e_{31}^{i*}}{\epsilon_3^{i*}} w'' \quad (6)$$

$$\bar{\varphi}_i = \varphi_i^+ - \varphi_i^-, \quad \tilde{\varphi}_i = \frac{\varphi_i^+ + \varphi_i^-}{2}$$

where φ_i^+ and φ_i^- are the subscribed electric potentials on the upper and lower skins of the i th surface layer. Notice that the electric potential is found to be the sum of a linear part, known from the applied uniform potentials φ_i^\pm , and a quadratic part, proportional to the beam curvature. This point is also true for thin piezoelectric plates¹⁴ and represents the induced potential, often neglected in the literature.

For the shear actuation mechanism $D_{C1,1}$ is neglected compared to $D_{C3,3}$, so that Eq. (5) still holds for the core. Its integration provides a linear potential in the core:

$$\varphi_C = \bar{\varphi}_C + z(\tilde{\varphi}_C/h_C) \quad (7)$$

where $\bar{\varphi}_C$ and $\tilde{\varphi}_C$ are the mean and relative potentials of the piezoelectric core.

Variational Formulation

The variational formulation of the adaptive piezoelectric sandwich beam can be expressed as

$$\delta T - \delta H + \delta W = 0, \quad \forall \delta \bar{u}, \delta \tilde{u}, \delta w, \delta \tilde{\varphi} \quad (8)$$

where δT , δH , and δW are the virtual variations of kinetic energy, electromechanical energy, and work done by applied mechanical loads, respectively. Each of these quantities can be expressed in terms of the main variables, namely \bar{u} , \tilde{u} , and w , for an actuation problem. However, for a sensing problem, $\tilde{\varphi}_i$ should be retained as a main variable.

Starting from the electromechanical energy of a piezoelectric medium, using constitutive equation (3) and (4) strain displacements and electric field-potential relations, and integrating through the thickness of the sandwiched beam leads to the following expression of δH :

$$\delta H = \delta H_F + \delta H_C \quad (9)$$

where δH_F and δH_C are the variations of the electromechanical energy corresponding to the surface layers and core layer, respectively. These are in turn decomposed into mechanical, piezoelectrical, and dielectrical contributions. Hence, δH_F takes the form

$$\delta H_F = \delta \bar{H}_{Fm} + \delta H_{Fme} + \delta H_{Fem} + \delta H_{Fe} \quad (10)$$

where

$$\begin{aligned} \delta \bar{H}_{Fm} &= \int_0^L \left\{ \left[(c_{11}^{A*} A_A + c_{11}^{B*} A_B) \tilde{u}' + (c_{11}^{A*} A_A - c_{11}^{B*} A_B) \frac{\tilde{u}'}{2} \right] \delta \tilde{u}' \right. \\ &\quad + \left[(c_{11}^{A*} A_A - c_{11}^{B*} A_B) \tilde{u}' + (c_{11}^{A*} A_A + c_{11}^{B*} A_B) \frac{\tilde{u}'}{2} \right] \frac{\delta \tilde{u}'}{2} \\ &\quad \left. + (\bar{c}_{11}^A I_A + \bar{c}_{11}^B I_B) w'' \delta w'' \right\} dx \\ \delta H_{Fme} &= \int_0^L \left[\left(e_{31}^{A*} A_A \frac{\tilde{\varphi}_A}{h_A} + e_{31}^{B*} A_B \frac{\tilde{\varphi}_B}{h_B} \right) \delta \tilde{u}' \right. \\ &\quad \left. + \left(e_{31}^{A*} A_A \frac{\tilde{\varphi}_A}{h_A} - e_{31}^{B*} A_B \frac{\tilde{\varphi}_B}{h_B} \right) \frac{\delta \tilde{u}'}{2} \right] dx \\ \delta H_{Fem} &= \int_0^L \left[\left(e_{31}^{A*} A_A \frac{\delta \tilde{\varphi}_A}{h_A} + e_{31}^{B*} A_B \frac{\delta \tilde{\varphi}_B}{h_B} \right) \tilde{u}' \right. \\ &\quad \left. + \left(e_{31}^{A*} A_A \frac{\delta \tilde{\varphi}_A}{h_A} - e_{31}^{B*} A_B \frac{\delta \tilde{\varphi}_B}{h_B} \right) \frac{\tilde{u}'}{2} \right] dx \end{aligned}$$

$$\delta H_{Fe} = \int_0^L \left(\epsilon_3^{A*} A_A \frac{\tilde{\varphi}_A}{h_A} \frac{\delta \tilde{\varphi}_A}{h_A} + \epsilon_3^{B*} A_B \frac{\tilde{\varphi}_B}{h_B} \frac{\delta \tilde{\varphi}_B}{h_B} \right) dx$$

$$\tilde{c}_{11}^i = c_{11}^{i*} + \frac{(\epsilon_{31}^{i*})^2}{\epsilon_3^{i*}}, \quad i = A, B$$

The core's contribution to the electromechanical energy variation of the sandwich beam can be written as

$$\delta H_C = \delta H_{Cm} + \delta H_{Cme} + \delta H_{Cem} + \delta H_{Ce} \quad (11)$$

where

$$\delta H_{Cm} = \int_0^L \left\{ c_{33}^{C*} A_C (\tilde{u}' + d w'') (\delta \tilde{u}' + d \delta w'') \right. \\ \left. + c_{33}^{C*} I_C \left(\frac{\tilde{u}'}{h_C} + \lambda w'' \right) \left(\frac{\delta \tilde{u}'}{h_C} + \lambda \delta w'' \right) \right. \\ \left. + c_{55}^C A_C \left[\frac{\tilde{u}}{h_C} + (\lambda + 1) w' \right] \left[\frac{\delta \tilde{u}}{h_C} + (\lambda + 1) \delta w' \right] \right\} dx$$

$$\delta H_{Cme} = \int_0^L e_{15}^C A_C \frac{\tilde{\varphi}_C}{h_C} \left[\frac{\delta \tilde{u}}{h_C} + (\lambda + 1) \delta w' \right] dx$$

$$\delta H_{Cem} = \int_0^L e_{15}^C A_C \left[\frac{\tilde{u}}{h_C} + (\lambda + 1) w' \right] \frac{\delta \tilde{\varphi}_C}{h_C} dx$$

$$\delta H_{Ce} = \int_0^L \epsilon_1^C A_C \frac{\tilde{\varphi}_C}{h_C} \frac{\delta \tilde{\varphi}_C}{h_C} dx$$

where I_i , A_i , $i = A, B, C$ are moment area and area of the i th layer. Notice that the piezoelectric material has a passive effect on piezoelectric layers through augmentation of their bending stiffness \tilde{c}_{11}^{i*} because of the induced potential effect.

For actuation problems, $\tilde{\varphi}_i$ are known (prescribed); hence, their virtual variations $\delta \tilde{\varphi}_i$ vanish. Consequently, δH_{em} and δH_e of Eqs. (10) and (11) also vanish. For the extension actuation mechanism, δH_{Cme} also vanishes because the core is elastic, and the variational equation (8) reduces for $\delta W = 0$ to

$$\delta \tilde{H}_{Fm} + \delta H_{Cm} - \delta T = -\delta H_{Fme} \quad (12)$$

Similarly, the shear actuation problem is obtained from Eq. (8) by

$$\delta \tilde{H}_{Fm} + \delta H_{Cm} - \delta T = -\delta H_{Cme} \quad (13)$$

where δH_{Fm} is similar to $\delta \tilde{H}_{Fm}$ but with $\tilde{c}_{11}^i = c_{11}^{i*}$.

From Eqs. (10) and (11) δH_{me} terms in Eqs. (12) and (13) can be interpreted as works of initial electric stresses. They also can be seen as works of actuation forces and moments. Hence, δH_{Cme} can be interpreted as an actuation-distributed sliding shear moment $e_{15}^C A_C (\tilde{\varphi}_C / h_C)$ induced by the applied electric potential $\tilde{\varphi}_C$ to the core layer. The conjugate displacement parameter is the sliding shear angle $(\tilde{u} / h_C) + (\lambda + 1) w'$. Interpretation of δH_{Fme} can be seen better in the practical case of identical surface layers. In this case

$$\delta H_{Fme} = \int_0^L \left(e_{31}^{F*} A_F \frac{\tilde{\varphi}_A + \tilde{\varphi}_B}{h_F} \delta \tilde{u}' + e_{31}^{F*} A_F \frac{\tilde{\varphi}_A - \tilde{\varphi}_B}{h_F} \frac{\delta \tilde{u}'}{2} \right) dx \quad (14)$$

Depending on the imposed potentials on the faces, two particular cases could be considered.

1) $\tilde{\varphi}_A = \tilde{\varphi}_B = \tilde{\varphi}_F$, for which δH_{Fme} reduces to

$$\delta \tilde{H}_{Fme} = 2 \int_0^L e_{31}^{F*} A_F \frac{\tilde{\varphi}_F}{h_F} \delta \tilde{u}' dx \quad (15)$$

For homogeneous material properties in the axial direction and uniform applied potentials, Eq. (15) becomes

$$\delta \tilde{H}_{Fme} = 2e_{31}^{F*} A_F (\tilde{\varphi}_F / h_F) \delta \tilde{u}(L) - 2e_{31}^{F*} A_F (\tilde{\varphi}_F / h_F) \delta \tilde{u}(0) \quad (16)$$

In this form $\delta \tilde{H}_{Fme}$ is interpreted as a virtual work of boundary actuation tractions $2e_{31}^{F*} A_F (\tilde{\varphi}_F / h_F)$ induced by the applied identical potentials on the surface layers. Only axial mean displacement or strain is produced.

2) $\tilde{\varphi}_A = -\tilde{\varphi}_B = \tilde{\varphi}_F$, and here δH_{Fme} reduces to

$$\delta \tilde{H}_{Fme} = \int_0^L e_{31}^{F*} A_F \frac{\tilde{\varphi}_F}{h_F} \delta \tilde{u}' dx \quad (17)$$

Again, this expression is integrated to obtain

$$\delta \tilde{H}_{Fme} = e_{31}^{F*} A_F (\tilde{\varphi}_F / h_F) \delta \tilde{u}(L) - e_{31}^{F*} A_F (\tilde{\varphi}_F / h_F) \delta \tilde{u}(0) \quad (18)$$

$\delta \tilde{H}_{Fme}$ is interpreted as a virtual work of the boundary actuation tractions $e_{31}^{F*} A_F (\tilde{\varphi}_F / h_F)$ induced by the applied identical but opposite potentials on the surface layers. Only axial relative displacement or strain of the surface layers is produced.

Comparing expressions of δH_{Cme} given in Eq. (11) to those of $\delta \tilde{H}_{Fme}$ in Eq. (16) and $\delta \tilde{H}_{Fme}$ in Eq. (18), an important feature can be noticed. That is, the extension actuation mechanism produces boundary forces (tractions/compressions), whereas the shear actuation mechanism induces distributed moments. The latter avoids the common singularity problems at the boundary of conventional extension actuators.

Variation of the kinetic energy of the sandwich beam is the same for both mechanisms and can be written in terms of the main variables as

$$\delta T = \int_0^L \left\{ \left[(\rho_A A_A + \rho_B A_B + \rho_C A_C) \ddot{u} + (\rho_A A_A - \rho_B A_B) \frac{\ddot{u}}{2} \right. \right. \\ \left. \left. + \rho_C A_C d \ddot{w}' \right] \delta \tilde{u} + \left[(\rho_A A_A - \rho_B A_B) \ddot{u} \right. \right. \\ \left. \left. + \left(\rho_A A_A + \rho_B A_B + 4\rho_C \frac{I_C}{h_C^2} \right) \frac{\ddot{u}}{2} + \rho_C \frac{I_C}{h_C} \lambda \ddot{w}' \right] \frac{\delta \tilde{u}}{2} \right. \\ \left. + (\rho_A A_A + \rho_B A_B + \rho_C A_C) \ddot{w} + \left[\rho_C A_C d \ddot{u} + \rho_C I_C \lambda \frac{\ddot{u}}{h_C} \right. \right. \\ \left. \left. + (\rho_A I_A + \rho_B I_B + \rho_C A_C d^2 + \rho_C I_C \lambda^2) \ddot{w}' \right] \delta w' \right\} dx \quad (19)$$

where ρ_i is the mass density of the i th layer.

Finite Element Discretization

Because \tilde{u} and \tilde{u} are C^0 -continuous and w is C^1 -continuous, they are interpolated by Lagrange linear and Hermite cubic shape functions, respectively. Classical FE procedure is followed to discretize actuator variational problems (12) and (13). Hence, the discretized shear actuation variational problem is

$$M \ddot{q} + (K_F + K_C) q = -F_{Ce} \quad (20)$$

where $q = [\tilde{u}_1, \tilde{u}_1, w_1, w_1', \tilde{u}_2, \tilde{u}_2, w_2, w_2']$ is the degree of freedom vector. M is the mass matrix of the sandwich beam obtained from the discretization of Eq. (19). K_F and K_C are the surface layers and core stiffness matrices obtained from the discretization of δH_{Fm} (with $\tilde{c}_{11}^i = c_{11}^{i*}$) and δH_{Cm} given in Eqs. (10) and (11), respectively. F_{Ce} is the induced electric load vector deduced from discretization of δH_{Cme} given in Eq. (11).

Discretization of the variational problem (12) leads to the following linear system:

$$M \ddot{q} + (\bar{K}_F + K_C) q = -F_{Fe} \quad (21)$$

where \bar{K}_F is the stiffness matrix of the piezoelectric surface layers and F_{Fe} is the induced electric force vector obtained from the discretization of δH_{Fme} [Eq. (10)].

Mass and stiffness matrices and mechanical and induced electric load vectors were integrated exactly, i.e., analytically. The present FE model was implemented on MATLABTM software. Good results have been obtained even for thin cores, indicating that the present element is shear locking free.

Analytic and Numerical Validation

A sandwich-beam FE capable of treating both shear and extension actuation mechanisms was implemented. To validate it, comparisons between present element results and analytical and numerical results found in the literature were made. Analytical and numerical results for static actuation of continuous⁸ and segmented⁷ configurations of cantilever beams were presented by Sun and Zhang.^{7,8} Modal analysis of segmented configuration of cantilever beams was presented by Lin et al.¹⁵ For all cases in the extension actuation mechanism, top and bottom layers are supposed to be PZT5H piezoelectric material, and the central core is supposed to be aluminum. For the shear actuation mechanism, top and bottom layers are assumed to be aluminum, and the central core is assumed to be composed of a small patch of PZT5H piezoelectric material and, covering the rest of the core, a rigid foam material.

Static Analysis

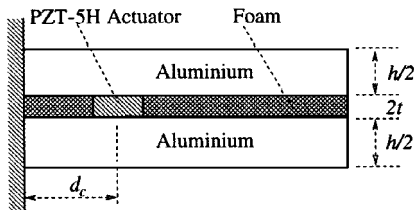
The segmented geometric configurations of both actuation mechanisms are presented in Fig. 1 with $L = 100$ mm, $h = 16$ mm, and $t = 1$ mm. The length and position of the actuator are $a = 10$ mm and $d_c = 15$ mm, unless stated differently. Beams are clamped at $x = 0$ and free at $x = L$. To bend the beam, voltages are applied at the top and bottom surfaces of piezoelectric layers, inducing bending electric forces. Material data are those given by Sun and Zhang.^{7,8} For the shear actuation mechanism, voltage applied to the piezoelectric core has a value of $\tilde{\varphi}_c = 20$ V, and for the extension actuation mechanism, voltages applied to surface actuators are $\tilde{\varphi}_F = 10$ V.

As a first analysis, the deflection of both beams for the continuous case, i.e., with actuators having the beam's length, was evaluated and compared to analytical results of Zhang and Sun⁸ to examine the convergence of the present element. In this case for the shear actuation mechanism, there is no rigid foam because the piezoelectric actuator occupies all of the core layer.

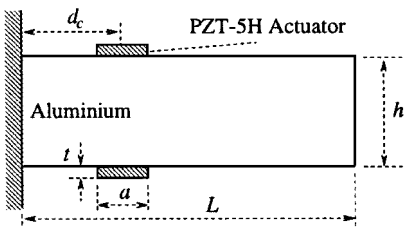
For both mechanisms the deformation of the continuous actuated cantilever beam was computed by only four FEs. Comparisons of these results to the analytical solution⁸ are represented in Figs. 2 and 3, indicating that FE results for the deflection of the shear and extension actuated beam match very well with the theoretical solution.⁸

The convergence of the element to the reference tip's displacement⁸ is shown in Fig. 4 for the shear actuation mechanism. For the extension actuation mechanism the FE produced errors of less than 0.05% for the beam's deflection. It is clear that the present element is very precise even with the low number of elements (less than 2% for two elements), and it converges monotonically and rapidly to the desired tip's deflection.

As a second analysis, the actuator's position is set to vary. In each case the shear actuated beam's tip displacement induced by applied electric forces is evaluated. The actuator's length is fixed at



a) Shear actuation configuration



b) Extension actuation configuration

Fig. 1 Segmented configurations of a cantilever sandwich beam for shear and extension actuation mechanisms.

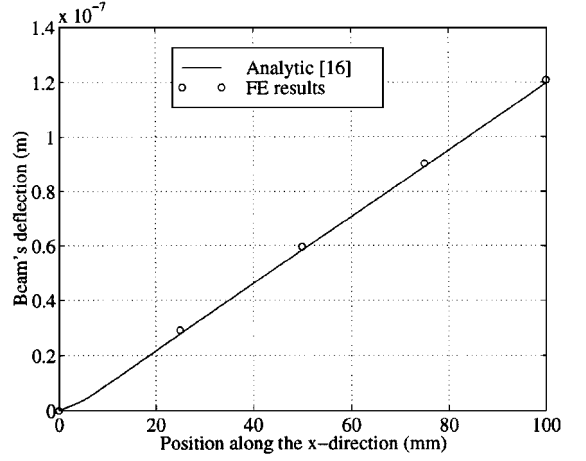


Fig. 2 Beam's deflection for shear actuation mechanism.

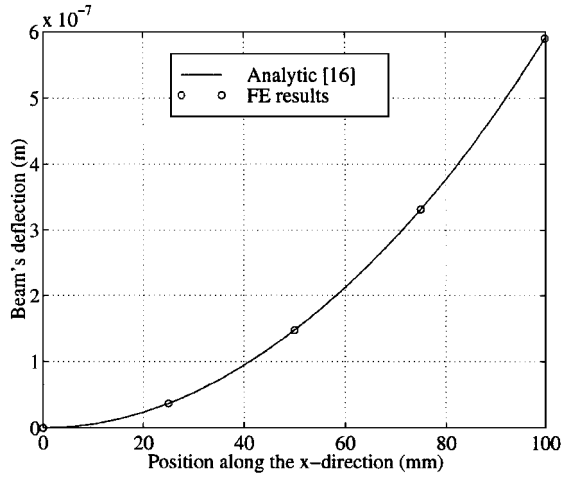


Fig. 3 Beam's deflection for extension actuation mechanism.

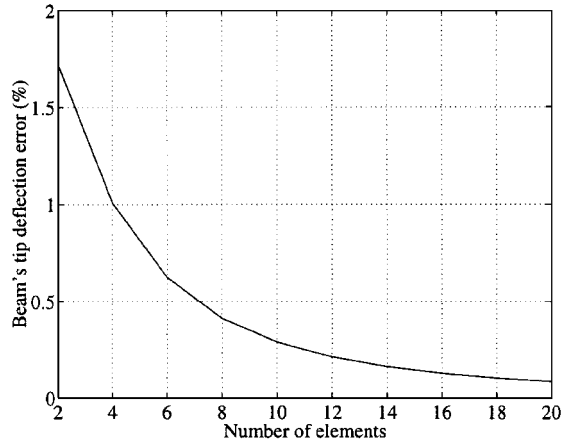


Fig. 4 Convergence of the beam's tip deflection for the shear actuation mechanism.

$a = 10$ mm, and the actuator's position is set to vary in the range 10–90 mm. The results shown in Fig. 5 indicate that the present FE results show very good agreement with the FE results presented by Sun and Zhang,⁷ using a commercial FE code. As expected, the actuator is more effective when close to the fixed end.

As piezoelectric actuation is applied in practice to different kinds of structures, it is worthwhile to investigate the effect of the structure's stiffness on the performance of the actuator. Therefore, an analysis of this effect was achieved by an evaluation of the beam's tip displacement through piezoelectric actuation for several structure stiffness ratios (Fig. 6). These ratios are defined as c_{11}^*/c_{33}^* for the

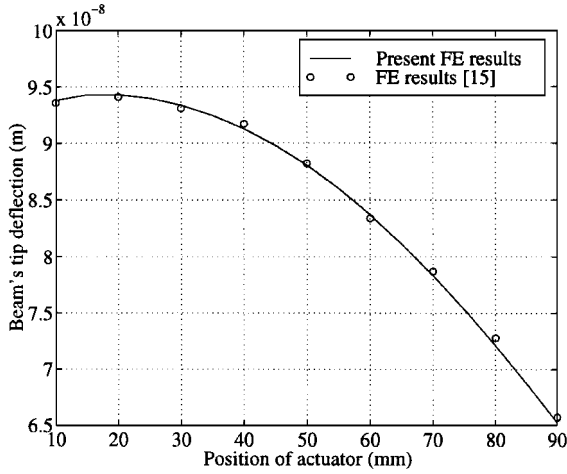


Fig. 5 Variation of the beam's tip deflection with the position of the actuator.

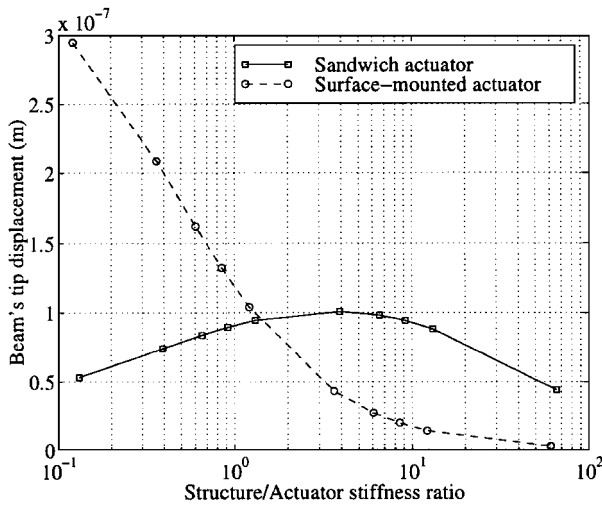


Fig. 6 Variation of the beam's tip deflection with the structure/actuator stiffness ratio.

shear actuation mechanism and c_{33}^*/c_{11}^* for the extension actuation mechanism. As can be seen in Fig. 6, the surface-mounted actuator is more efficient when its stiffness is greater than the structure's one. Nevertheless, although the sandwich actuators are not as efficient in this case, they preserve their effectiveness in the entire range, especially in the most common structure/actuator stiffness ratio range between 1 and 10. This is a great advantage for the shear actuation mechanism because, in contrast to the extension one, its performance is preserved for stiffer structures. Figure 6 shows also that there is an optimal stiffness ratio range for which the shear actuation mechanism is always better than the extension one, which is the case for PZT5H and the faces' stiffer material.

The variation of the beam's tip deflection with the actuator's thickness was also evaluated. In Fig. 7 the shear actuation mechanism is more performant than the extension one for thicker actuators, as can be expected. Therefore, for the case presented the extension actuation mechanism is more efficient in a low range ($t < 2$ mm), whereas, as noticed from Fig. 7, for $t > 2$ mm the shear actuation mechanism tends to be more efficient than the extension one.

Free-Vibration Analysis

Natural modes and frequencies were evaluated for both shear and extension actuation mechanisms. Material data are the same as presented by Lin et al.,¹⁵ and geometric parameters are $L = 50$ mm, $h = 2$ mm, $t = 0.5$ mm, $d_c = 11$ mm, and $a = 20$ mm. The first five natural frequencies are given in Table 1 for both actuation mechanisms. Table 1 shows that the natural frequencies of the shear actuated beam are lower than those of the extension actuated one, which can be explained by the fact that the sandwich configuration is less

Table 1 First five natural bending frequencies (Hz) and shear and extension actuated cantilever beam

Mechanism	1	2	3	4	5
Shear actuation	985	3,912	8,305	17,273	25,980
Extension actuation	1,084	4,787	12,422	24,547	38,599
Analytical results ¹⁵	1,030	4,230	12,000	23,500	38,500

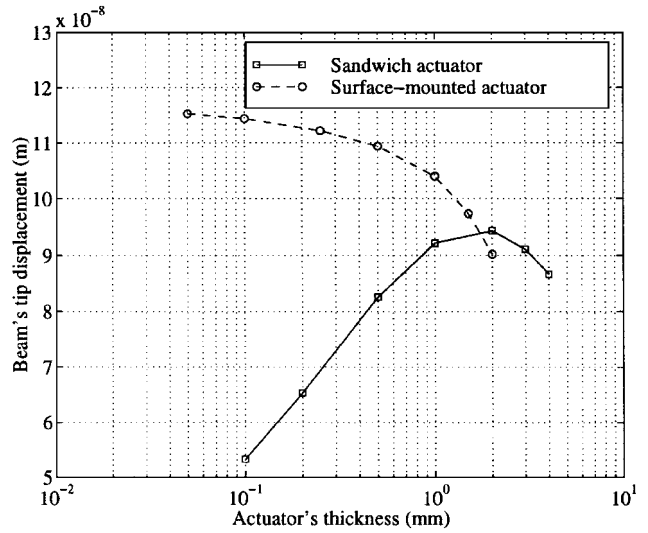


Fig. 7 Variation of the beam's tip deflection with the actuator thickness.

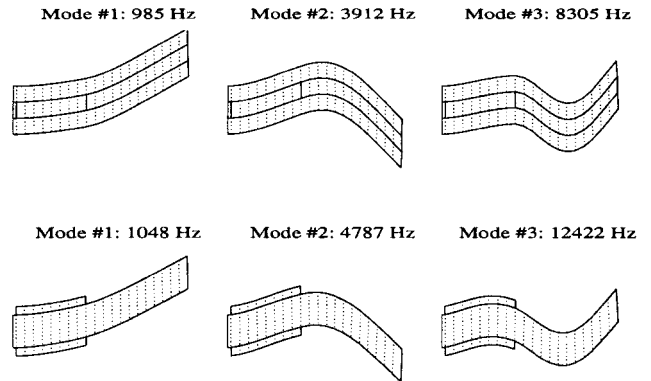


Fig. 8 Bending vibration modes for shear and extension actuation mechanisms.

rigid than the extension configuration because of the presence of the foam in the core. This difference increases with frequency because the foam becomes more deformed (Fig. 8). In all three bending modes the actuator's deformation is lower for the shear actuation mechanism. Analytic frequencies were given only for the extension actuation mechanism because there were not any in the literature for the shear actuation mechanism. Our values for the latter mechanism are given in Table 1 for future reference.

Conclusions

A theoretical formulation and FE implementation of a new adaptive asymmetric sandwich beam model were presented and validated for both extension and shear actuation mechanisms. Mechanically, the model is based on Bernoulli-Euler assumptions in the faces and Timoshenko hypotheses in the core. Rotatory inertia effects were considered for all layers. Electrically, the electric potential was found to be quadratic for the extension actuation mechanism (piezoelectric faces) and linear for the shear actuation mechanism (piezoelectric core). Besides, the sandwich beam was supposed to be short-circuited, i.e., electric potentials were imposed on upper and lower faces of piezoelectric layers, and natural boundary conditions (free-charge) were assumed on the remaining lateral boundaries.

A first adaptive sandwich-beam model was developed in previous works.^{9,11} Because of the presence of shear-locking problems in this element, a second model with a different kinematics description was developed here. This second adaptive sandwich-beam model, taking into account the extra shear because of the sliding of the faces against the core, also allowed a better understanding of the energy-dissipation capacity of the beam.

Theoretical and numerical comparisons of shear and extension actuation mechanisms for statics and vibration of smart beams were presented. The present results matched better with the analytical results than the results of the previous element, showing better convergence characteristics. Thanks to the new kinematics description, the new adaptive beam element did not present shear-locking problems. Surface-mounted actuators, acting through the e_{31} piezoelectric constant, induce boundary concentrated forces and moments in the structure, whereas sandwich shear actuators, acting through the e_{15} piezoelectric constant, induce distributed moments in the structure. Therefore, we can expect fewer problems of the actuators' debonding at its extremities for the shear actuation mechanism.

Comparisons between both actuation mechanisms in static piezoelectric actuation showed that only thin extension actuators are efficient. Shear actuators, on the contrary, are more effective for a medium thickness range. Shear actuators' performance is less dependent on the structure's stiffness. Moreover, for rigid structures the shear actuation mechanism presents better performance than the extension one.

Vibration analysis of both actuation mechanisms was presented through evaluation of natural bending frequencies and modes. Vibration modes are equivalent in both mechanisms; nevertheless, shear actuators are less deformed than extension ones, and natural frequencies are higher for the extension actuation mechanism.

The present work is being extended to implement the sensing capacity of the adaptive sandwich beam to study active control applications.

References

- ¹Hagood, N. W., Kindel, R., Ghandi, K., and Gaudenzi, P., "Transverse Actuation of Piezoceramics Using Interdigitated Surface Electrodes," *North American Conference on Smart Structures and Materials*, Vol. 1917, Society of Photo-Optical Instrumentation Engineers, Albuquerque, NM, 1993, pp. 341–352 (SPIE Paper 1917-25).
- ²Aldraihem, O. J., and Wetherhold, R. C., "Mechanics and Control of Coupled Bending and Twisting Vibration of Laminated Beams," *Smart Materials and Structures*, Vol. 6, No. 2, 1997, pp. 123–133.
- ³Bent, A. A., Hagood, N. W., and Rodgers, J. P., "Anisotropic Actuation with Piezoelectric Fiber Composites," *Journal of Intelligent Materials Systems and Structures*, Vol. 6, No. 3, 1995, pp. 338–349.

⁴Han, T.-H., and Lee, I., "Active Damping Enhancement of Composite Plates with Electrode Design Piezoelectric Materials," *Journal of Intelligent Materials Systems and Structures*, Vol. 8, No. 3, 1997, pp. 249–259.

⁵Bent, A. A., and Hagood, N. W., "Piezoelectric Fiber Composites with Interdigitated Electrodes," *Journal of Intelligent Materials Systems and Structures*, Vol. 8, No. 11, 1997, pp. 903–919.

⁶Soong, T. T., and Hanson, R. D., "Recent Development in Active and Hybrid Control Research," *1st International Workshop on Structural Control*, edited by G. W. Housner and S. F. Masri, Univ. of Southern California, Los Angeles, CA, 1993, pp. 483–490 (Paper 46).

⁷Sun, C. T., and Zhang, X. D., "Use of Thickness Shear Mode in Adaptive Sandwich Structures," *Smart Materials and Structures*, Vol. 4, No. 3, 1995, pp. 202–206.

⁸Zhang, X. D., and Sun, C. T., "Formulation of an Adaptive Sandwich Beam," *Smart Materials and Structures*, Vol. 5, No. 6, 1996, pp. 814–823.

⁹Benjeddou, A., Trindade, M. A., and Ohayon, R., "A Finite Element Model for Extension and Shear Piezoelectrically Actuated Adaptive Structures," *Japan-France Seminar on Intelligent Materials and Structures*, Tohoku Univ., Sendai, Japan, 1997, pp. 277–295.

¹⁰Benjeddou, A., Trindade, M. A., and Ohayon, R., "A Finite Element Model for Shear Actuated Adaptive Structures," *8th International Conference on Adaptive Structures and Technologies*, edited by Y. Murotsu, C. A. Rogers, P. Santini, and H. Okubo, Technomic, Lancaster, PA, 1997, pp. 133–142.

¹¹Benjeddou, A., Trindade, M. A., and Ohayon, R., "A Unified Beam Finite Element Model for Extension and Shear Piezoelectric Actuation Mechanisms," *Journal of Intelligent Materials Systems and Structures*, Vol. 8, No. 12, 1997, pp. 1012–1025.

¹²Benjeddou, A., Trindade, M. A., and Ohayon, R., "Comparison of Extension and Shear Actuation Mechanisms for Smart Structure Beams," *4th European Conference on Smart Structures and Materials*, edited by G. R. Tomlinson and W. A. Bullough, Inst. of Physics, Bristol, England, UK, 1998, pp. 131–138.

¹³Kim, G., Jensen, T., DeGiorgi, V., Bender, B., Wu, C. C., Flipen, D., Lewis, D., Zhang, Q., Mueller, V., Kahn, M., Silberglett, R., and Len, L. K., "Composite Piezoelectric Assemblies for Torsional Actuators," U.S. Naval Research Lab. and Penn State Univ., Rept. NRL/MR/6380-97-7997, Washington, DC, Sept. 1997.

¹⁴Rahmoune, M., Osmont, D., Benjeddou, A., and Ohayon, R., "Finite Element Modeling of a Smart Structure Plate System," *7th International Conference on Adaptive Structures and Technologies*, edited by P. Santini, C. A. Rogers, and Y. Murotsu, Technomic, Lancaster, PA, 1996, pp. 463–473.

¹⁵Lin, M. W., Abatan, A. O., and Rogers, C. A., "Application of Commercial Finite Element Codes for the Analysis of Induced Strain-Actuated Structures," *2nd International Conference on Intelligent Materials*, edited by P. C. A. Rogers and G. G. Wallace, Technomic, Lancaster, PA, 1994, pp. 846–855.